

Classification and study of near-surface region of active material for gas detection using x-ray photoelectron spectroscopy

Pravin S. More^{1*}, Dattatray J. Late², Subhash B. Kondawar³

¹Department of Physics, Institute of Science, Madam Kama Road, Fort Mumbai 400032, India

²Physical and Materials Chemistry Division, CSIR-National Chemical Laboratory, Pune 411 008, India

³Department of Physics, Rashtrasant Tukadoji Maharaj Nagpur University, Nagpur 440033, India

*Corresponding author. E-mail: psmore.ism@gmail.com

Received: 03 September 2015, Revised: 01 December 2015 and Accepted: 03 January 2016

ABSTRACT

We report investigations on resistive material SnO₂: Cu (9 wt. %) evaluated and optimized for the application of gas sensor. SnO₂: Cu has been thoroughly characterized by using X-ray photoelectron spectroscopy (XPS). The deconvolution of XPS spectra confirms the existing surface reactive species in the form of states of the metal orbital and the presence of multiple pathways for the detection of CO vis-à-vis sintering temperature effect. Enhanced CO pickup at the sintering temperature of 650 °C (wide range and low sensitivity) and 750 °C (short range and high sensitivity) has been observed. The CO sensing and XPS data correlates well along with the nonconventional use of variation in average XPS background intensity of general scan seems to be related to optimized sensitivity conditions of various gases. Copyright © 2016 VBRI Press.

Keywords: Resistive material; SnO₂; sintering temperature; X-ray photoelectron spectroscopy.

Introduction

Semiconducting oxide nanomaterial-based gas sensors have been utilized for a variety of applications including industrial emission control, medical diagnosis, civil life, and environmental monitoring. The development of miniaturized, low-cost sensor device techniques is important to make gas sensors commonly accessible for variety of applications. In particular for indoor and outdoor air quality monitoring, medical diagnostics and food quality control requires small and low-cost gas sensors. Carbon dioxide (CO) sensors can be used in vehicles interiors or in the air-conditioned buildings. Oxygen sensors can be used to monitor the ignition in engines and power plants and the methane gas sensors can be used to identify gas leaks. The sensors in intelligent food packaging can recognize if the meat or fish is still fresh or not. Furthermore, number of diseases can be detected by analyzing trace gases in exhaled breath. The use of sensors in various applications has the advantage for relevant signal that can be easily detected and recorded. The sensor that is investigated in this manuscript was based on two terminal devices which act as a micro-electronic switch. An interesting application area of oxide based sensors is the detection of various gases such as nitrogen oxides (NO_x). Nitrogen oxides are generated due to the combustion of fossil fuels which play important role in formation of ozone, acid rain and fog. The NO₂ gas is the indicator of larger group of NO_x and is the module of greatest interest because of its inhalation leads to respiratory problems, such as airway inflammations. Real-

time monitoring of NO₂ is very important for public health and environmental protection.

The surface electronic structural properties of metal-oxides nanostructures play an important role in their use in many technologically important areas such as catalysis, chemical gas sensing and micro/nanoelectronics. The variety of metal oxide nanomaterials with various morphology such as ZnO, SnO₂, Fe₂O₃, MoO₃, CuO, NiO, V₂O₅, TiO₂ and their composites materials like Pt/SnO₂, Pt/ZnO, Pd/SnO₂ has been found to be superior in sensing applications with fast response and recovery time as well [1-13]. The advantage of metal oxide nanomaterials are their low cost, highly robustness and highly sensitivity and selectivity.

Recently variety of morphology synthesized for sensing performance which includes nanowires, nanorods, nanosheets and nano flowers etc [14-17].

The SnO₂ has a tetragonal structure with lattice parameters of $a = b = 4.737\text{\AA}$ and $c = 3.816\text{\AA}$. [18] The undistorted system has regular octahedron co-ordination in which one tin (Sn) atom is surrounded by six oxygen (O) atoms. At room temperature it has a band gap of 3.6 eV. [19] The unique optical, electrical and magnetic properties of SnO₂ system have generated an enormous interest for its use [20]. Researchers are actively trying to achieve different morphology of SnO₂ because with the change in surface morphology, the surface reactivity changes which ultimately affect the properties like electrical, optical, and magnetic properties. Systematic emergence of inherent surface states and extrinsic defects state are therefore

fundamental and of practical interest for different applications such as gas sensor. The surface properties of SnO₂:Cu, SnO₂:CuO, ZnO:CuO, etc. were investigated in terms of chemical (gas) sensing activity [21-25].

Present investigations deals with surface characterization and effect of oxygen at different sintering temperatures (600-800 °C) in SnO₂: Cu pellets. The SnO₂:Cu surfaces were studied using XPS and XRD to know the surface and interface interaction of Cu with SnO₂ and electrical properties of SnO₂:Cu material. Further, the operational mechanisms of NO_x detection with electron transition were investigated and are used to develop a sensitive real-time NO₂ sensor.

Experimental

Material synthesis

In present study the commercially available nano-structure SnO₂ (tetrahedral coordinated) powder (Thomas Baker, 99.9 %) with optimized 9 wt. % Cu powder was thoroughly mixed in acetone medium and dried in ambient air. Above mixture is sintered at different temperatures and subsequently pulverized to get fine powder. The powder is than cold-pressed (5 tone) to form pellet (13 mm diameter) by mixing it with 3 wt. % polyvinyl alcohol (PVA). The pellets are then fired at 300 °C in ambient air to burn out PVA. The average thickness of the pellet was about 1.2 mm.

Characterizations

In the present system ESCA 3000 electron spectrometer with non-monochromatic (200W), Mg K α (1253.6 eV) was used to characterize the surface of the samples. The vacuum in the analyzer was used to detect the photoelectron energy state. The XPS spectrum was acquired at 50 eV pass energy, with 5mm slit width and at normal incidence angle. The spectrometer was calibrated by determining the binding energy value of Au 4f_{7/2} line at 84 eV [33-35, 37-39]. XPS instrumental resolution obtained under this condition is 1.0 eV {full widths at half maxima (FWHM) for the Au4f_{7/2} level [40, 41] the compound structure was confirmed by X-ray diffraction using ['Phillips', Model 1729] X-ray diffractometer (Cu K α λ =1.5406 Å). Energy dispersive X-ray analysis (EDAX) study was also carried out for elemental analysis (Leica 440 Model). The XPS spectrum of SnO₂: Cu samples in the form of pellets [21-23] sintered at various temperature from 600 °C to 800 °C were recorded. X-Ray photoelectron spectroscopy (XPS) measurements were carried out for mixed metals and metal oxide which shows the presence of multivalent oxygen species on the surface. Due to its surface sensitive nature and non- deification (degradable) nature of the surface the XPS is used to distinguish the different species formed during the surface dispensation, segregation and through the defect chemistry can be described consistently by assuming fully ionized oxygen vacancies and conduction electrons as native defect. The oxygen non-stoichiometry is also one of the causes of instability in the electrical behavior of tin dioxide and copper oxide pellets. In the sintering / annealing processes the oxygen molecule interact and diffuses in to SnO₂ [26-34] / CuO [35]. The atomic state like lattice oxygen, carbonates oxygen, hydroxide and

oxygen contain impurities such as O²⁻, O⁻, O₂²⁻ ions [36, 37] and adsorbed atomic oxygen. Due to the surface sensitive nature of the XPS it is possible to study the surface oxidation states, surface pore formation and the formation of intermediate complex due to the metal oxides/metal oxide interaction, grain boundaries etc. These properties are related to kinetic mechanisms of the gas sensing.

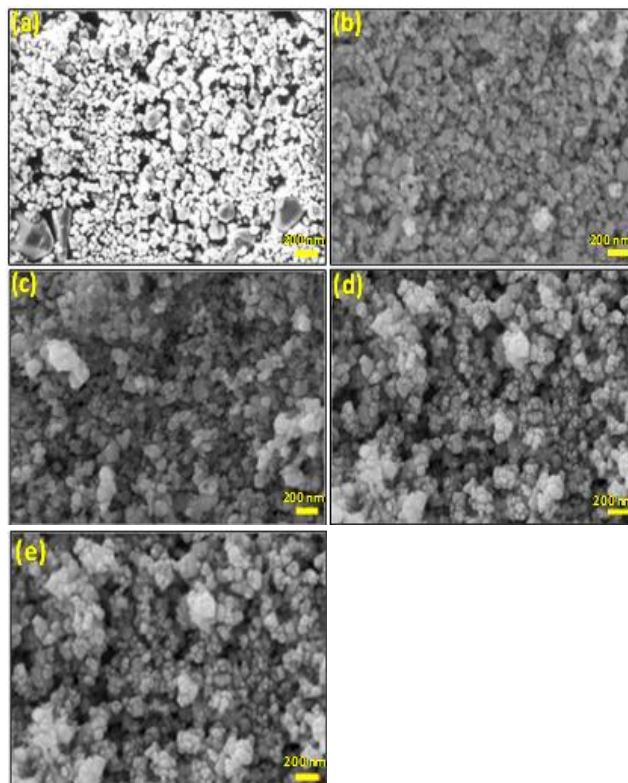


Fig. 1. SEM images of SnO₂ micro/ nano particles pellet sintered at (a) 600°C, (b) 650°C, (c) 700°C, (d) 750°C (e) 800°C.

Results and discussion

Fig. 1 shows the SEM images of SnO₂ micro / nano power pellet sintered at various temperatures. The SEM images clearly demonstrate an increase in the grain growth. The presence of Cu in SnO₂ can form a series of inter-metallic phases. It is also known that substitution of Sn⁴⁺ by Cu²⁺ in SnO₂ increases concentration of "O" vacancies and decreases concentration of free electrons. Existence of cuprous ion (Cu⁺) due to partial reduction of Cu²⁺ during sintering /calcinations increases sensor response for NO and CO₂, H₂S, CO and H₂ [21-23]. **Fig. 3** gives typical survey scan of a sample of SnO₂:Cu pellet. In the survey scan data about 30 lines are observed which are given in **Table 1**. We have analyzed only for three selected high resolved lines of Sn, O and Cu (which are marked by * in the **Table 1**). XPS is taken only for SnO₂:Cu (Cu = 9 wt. %) pellets sintered at 600, 650, 700, 750 and 800 °C. As seen from **Fig. 3** there are about 30 lines which indicate that the Sn, Cu, O and C elements are present. However, there are only 25 lines in samples sintered (**Table 1**) at 650 and 750 °C. The sample sintered at 700 and 800 °C shows only 20 and 27 lines, respectively. The absent lines are also given in **Table 1**. It is clear from this data that the presence of CuO, Cu₂O and adsorbed O₂ at

700 and 800 °C. The T_{sinter} has reduced the number of lines (Sn as well as Cu elements) and it has probably quenched the SF value for H₂ and CO and (c) Cu₂O is present only for 800 °C sintered which is apparently useful for increase in LPG (liquefied petroleum gases) sensitivity (an LPG signature in XPS). We discussed more critical points below.

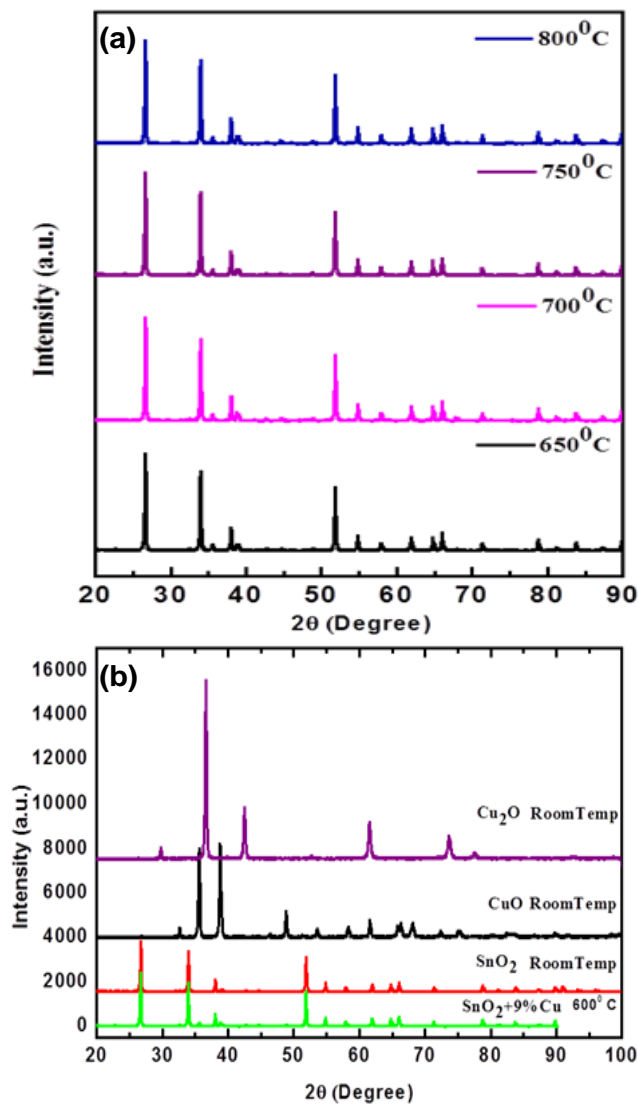


Fig. 2. The XRD pattern of various SnO₂:Cu pellets sintered at different sintering temperature with a comparison with pure SnO₂, CuO and Cu₂O.

Fig. 2 Shows XRD pattern for SnO₂:Cu pellet nano powder sintered at various temperatures. The selected region of X-RD pattern from 40-48° at various sintering temperature exhibits single-phase material with tetragonal symmetry. Furthermore, XRD patterns show additional reflections due to CuO and there is no reflections corresponding to Cu metal were observed. The reflection ($2\theta = 35.54^\circ$) corresponding to CuO was observed only in case of 9 and 11 wt. % of Cu with the monoclinic symmetry. The absence or low intensity of the reflection ($2\theta = 35.54^\circ$) of CuO corresponding to 1, 3, 5 and 7 wt. % of Cu may be due to the lower concentration of Cu. All the reflections are corresponding to only the tetragonal phase

of SnO₂ [JCPDS data card No. 21-1250]. In addition 2 or 3 reflections (at $2\theta = 35.54, 38.72, 48.76^\circ$) corresponding to the monoclinic phase of CuO [JCPDS data card no. 5-661] are also observed in all the XRD patterns. The intensity of the peaks corresponding to CuO peak goes on increasing slightly for sintering temperatures of 600 to 650 °C. Then it is nearly constant up to the sintering temperature of 800 °C. Further a very small peak at $2\theta = 42.60^\circ$ corresponding to the cubic Cu₂O phase [JCPDS card no. 34-1354] is also observed in the patterns for the pellets sintered at and above the 800 °C. Furthermore, resolved pattern shows a probable reflection of composite of SnO₂:Cu. The crystallite size for all the samples is calculated by using the Scherer equation. The average crystallite size of the samples sintered at 600, 650 and 750 °C for SnO₂:Cu system is 15-20 nm whereas for the samples sintered at 700 and 800 °C; the crystallite sizes are ≥ 30 nm.

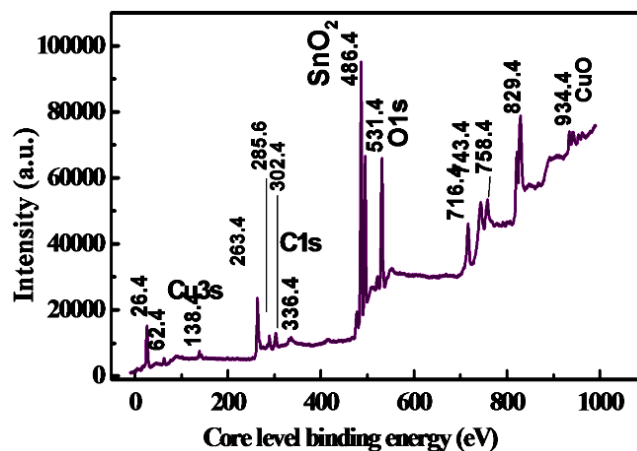


Fig. 3. The survey scan for SnO₂:Cu, Cu = 9 wt. % sample sintered at 600 °C.

Generally, it is well known that XPS patterns do contain carbon (For C 1s B.E. ~ 285.6 eV, **Fig. 3, 4** which is used as reference for BE shift for any specific line. This is followed in present work as well. High resolution expanded raw patterns of only a few selected lines give corresponding plots of variation of intensities (this can be related to CO and LPG optimum T_{sinter}) with sintering temperature. It can be seen from **Fig. 4(b)** that the intensities of Sn and O successively decrease up to 700 °C and then increase rapidly, while intensity of Cu element decreases gradually up to 750 °C and again increases at 800 °C. The deconvoluted patterns of most of the above related XPS samples are seen for Sn 3d core level particular to 700, 750 and 800 °C and the deconvoluted patterns for O 1s and Cu 2p respectively for 600, 650, 700, 750 and 800 °C samples. In all the cases, the notations of Sawatzky *et al.* [35] are followed [figures not shown]. Figure shows the Sn 3d_{5/2} orbital with deconvoluted components of Sn⁴⁺. The binding energy (B.E.) values agree with the literature [33, 34, 36, 37]. A small shift in peak of B.E. value is seen for samples sintered at 600, 650, 800 (lower B.E.) vis-à-vis 700, 750 °C (higher) with an identical shift in the O 1s spectrum. The O 1s spectrum shows 2 components. High resolution scans for Sn 3d, Cu 2p, and O 1s have been deconvoluted (decomposed) using both linear sub-routines (Microcal

Origin Commercial Software, Ver. 6.1). The shake up satellite (SUS) from fig 4a, for 800 °C data shows positive shift of ~3 eV and existence of structure for Cu 2p_{3/2} line which is shown by Sawatzky *et al.* [35, 36, 42, 43]. The presence of O⁻ species at the surface is an important pathway for catalysis reaction [38, 44]. The BE at 529 eV has been identified to bridging "O" on the surface [44] and also the presence of O⁻ and O²⁻ leads to depletion layer at surface of SnO₂ [44]. The peak at 532.6 eV corresponds to O₂²⁻ [38]. Sn₃O₄ is known to form between 250 and 525 °C [44]. The O₂⁻ and O⁻ form at the temperature of < 180°C and > 200 °C respectively [44]. These may have been responsible during sensor operation at the operating temperature.

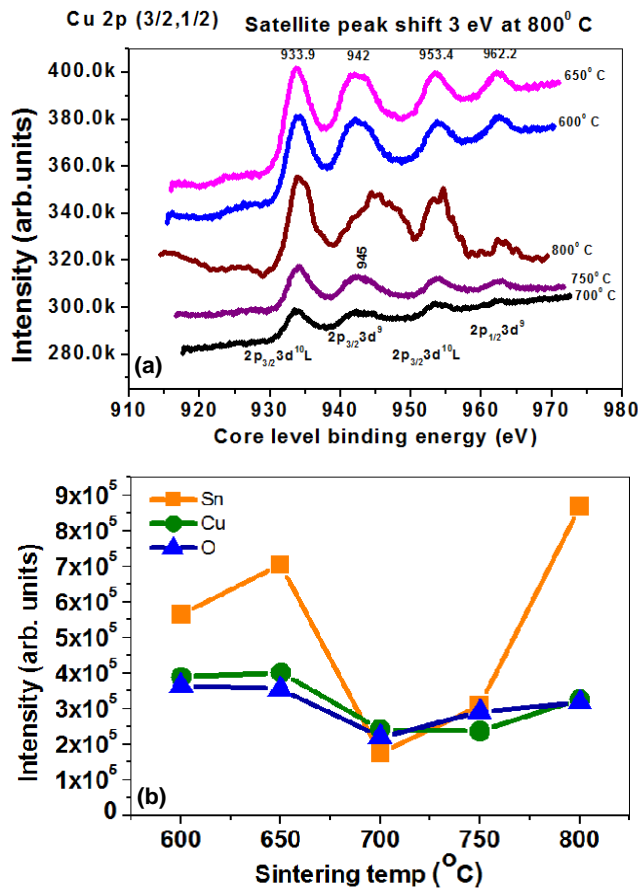


Fig. 4. (a) High resolution XPS spectra of selected regions for Cu 2p (3/2, 1/2) and (b) Variation of intensities of Sn 3d (3/2, 5/2), O 1s and Cu 2p (3/2, 1/2) with sintering temperature (T_{sinter}).

It is well known that XPS nonlinear background is mostly due to deep core level electrons and hence the above conventional analysis may not give, directly the resistive sensor relation (conventional band) information. On the other hand, the general background is expected to be mainly related to inelastic scattering by the other (outer) atomic electrons and band level electrons. Therefore this may also give some information about conduction band (& nearly donor /acceptor levels). We therefore decided to summarize these general scan through the general background. However, the relative change in slopes and appearance of new features will be sufficiently reliable.

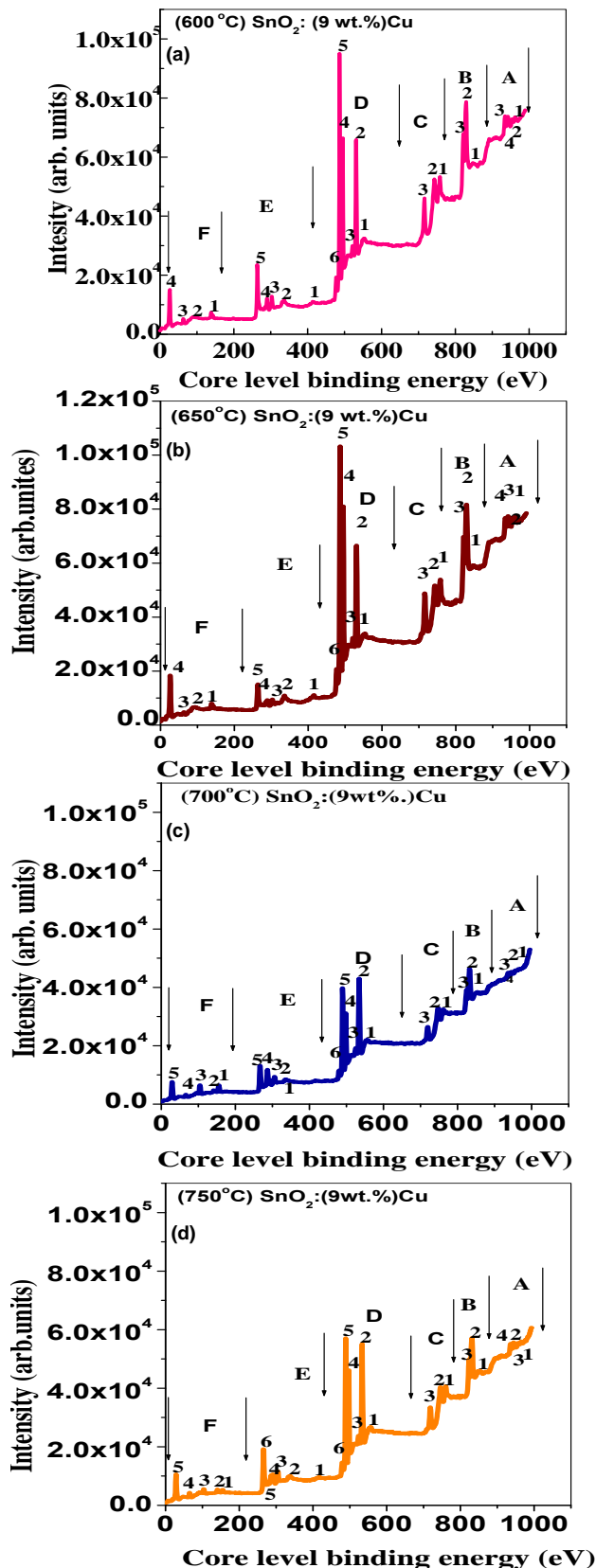


Fig. 5. (a-d): The full scan for samples of SnO₂:Cu, Cu = 9 wt. % sintered at 600, 650, 700 and 750°C it is divided into different parts/ranges: A, B, C, D, E and F each containing few intense peaks.

More importantly it was seen that the general trends in all the five sintered samples was the same as e.g. see in Fig. 5 gives six regions (A to F) with stepped background

structure. There are some overall changes with T_{sinter} e.g. The 600, 650 and 800 °C samples show higher intensities than 700, 750 °C samples, but this needs to be conformed and may not be very reliable observation. There are some relative changes given below, which are (being relative), reliable the end region of A (called as it is near 1000 eV) gives slightly rising slop for T_{sinter} 600 & 650°C & for 700, 750 °C it is very fast rising, but for 800 °C it becomes a falling slop [These can be signature of H₂, CO and LPG respectively].

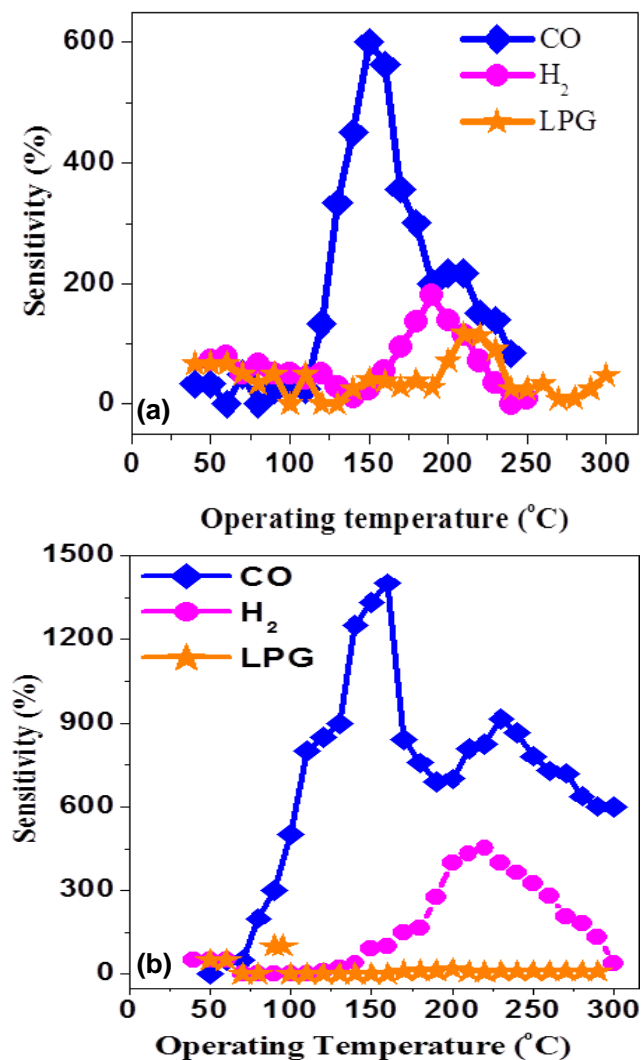


Fig. 6. Typical sensitivity factor for CO, H₂ and LPG at 1000 ppm with varying operating temperature for SnO₂:Cu (Cu = 9 wt. %) pellets sintered at (a) 650°C and (b) 750°C.

The slopes levels A₁, A₂ (just before A₅) behave in similar fashion as A₅ i.e. equal level at 600 & 650 °C, rising slope at 700, 750 °C. In region B (see **Fig. 5**) the BE levels B₁, B₂ have same amplitude at 600, 650, 800 °C but at 700, 750 °C Amplitude B₁ > B₂ rise at 600, 650 °C sub steps is similar at 700, 750 °C and at 800 °C it is somewhat falling sub steps. Peaks E5 (E4 & E6) are suddenly reduced at 650 °C from that of 600 °C, peak E4 splits into two & peaks E4 & E5 are absent at 800 °C. These critical changes at ~ 600, 750 and 800 °C can be possible signature in XPS (general background) for H₂, CO, LPG gases sensing. Of course

these are only indirect conclusions and not proved with any theoretical basis, we need to see the effect of wt. % of Cu (not studied), starting with pure SnO₂ for seeing Cu effects. This will give Cu signature and variations in it may related to Cu wt.% & sintering temperatures as well (the experiments which is not carried out even for sensor work with such various combinations of at Cu. % and T_{sinter}) given in **Table 1**.

Table 1. Experimental XPS survey scan data [Binding energy units (eV)] of all the samples sintered at 600, 650, 700, 750 and 800°C. Sn [39]: 1s², 2s², 2p⁶, 3s², 3p⁶, 4s², 3d¹⁰, 4p⁶, 5s², 4d¹⁰, 5p²; Cu [29]: 1s², 2s², 2p⁶, 3s², 3p⁶, 4s², 3d⁹; O [8]: 1s², 2s², 2p⁴; * Overlapping transition Cu L₂₃ M₂₃ M₂₃ and Sn 3d; O KVV and Sn 3p, O 2s and Sn 4d; Cu L₃M₂₃M₂₃ and Sn 3p; Auger transitions are given in kinetic energy (KE – eV) units; [?]: 62, 110, 160 and 260 transitions are not assigned.

Region	Lines in Fig. 5	B.E. (eV)	Intensity (arbs. Units)				Peak designation	
			650 °C	700 °C	750 °C	800 °C		
F	5	160	absent	absent	64k	49k	absent ?	
	4	26.4	15k	18k	76k	10k	O 2s	
	3	63.4	52k	48	28k	43k	?	
	2	91.4	59k	66	64k	55k	Sn 4p Broad band	
	1	138.4	74k	79	48k	54k	Sn 4s	
	6	286.4				10k	10k	C 1s
E	5	263.4	23k	45	12k	19k	?	
	4	289.4	12k	92	11k	10k	10k	C 1s
	3	302.4	12k	92	82k	11k		C 1s plasmon
	2	335.4	11k	10	93k	10k	11k	Cu LVV
	1	420.4	10k	11	84k	98k	10k	* Cu L ₂ M ₂₃ V * Cu L ₃ M ₂₃ V
D	6	477.4	19k	20	11k	14k	20k	?
	5	486.4	95k	10	39k	57k	118k	Sn 3d
	4	495.4	66k	81	31k	46k	931k	Sn 3d
	3	521.4	30k	32	19k	23k	36k	?
	2	531.4	65k	66	43k	55k	68k	O 1s
	1	552.4	32k	33	21k	26k	37k	*Cu L ₂ M ₄₅ M ₄₅ *Cu L ₃ M ₄₅ M ₄₅
C	4	779.4					53k	Sn 3p
	3	716.4	46k	48	26k	33k	54k	Sn 3p
	2	743.4	52k	51	33k	40k	57k	O KVV
B	1	758.4	53k	53	32k	40k	59k	Sn 3p
	3	821.4	67k	82	39k	48k	70k	Sn M ₂ N ₄₅ N ₄₅
A	2	829.4	78k	82	46k	57k	67k	
	1	847.4	58k	84	38k	45k	51k	?
	6	892.4					54k	Sn 3s
	5	937.4					59k	Cu 2p
	4	934.4	73k	93	45k	55k	57k	
	3	942.4	73k	94	44k	55k	57k	
	2	955.4	72k	95	45k	55k	56k	
	1	963.4	72k	96	46k	55k	54k	

Fig. 6. shows the typical Sensitivity for SnO₂:Cu (Cu = 9 wt. %) nano powder pellet operating at various temperature for CO, H₂ and LPG at 1000 ppm of gas for pellet sintered at (a) 650 °C and (b) 750 °C. As we can see the sintering temperature is very crucial for sensitivity. As in case CO gas sensitivity increases from ~ 600 % to ~ 1350 % as we increases the sintered temperature from 650 °C to 750 °C. One can also see the noticeable change in H₂ gas sensitivity also. But in case of LPG sensitivity factor found to be slightly decreases. In the presence of a reactive gas such as carbon monoxide, the surface catalyzed combustion $\text{CO} + \text{O}^{2-} \rightarrow \text{CO}_2 + 2e^-$ and $\text{H}_2 + \text{O}^{2-} \leftrightarrow \text{H}_2\text{O} + 2e^-$ may occur so that the surface coverage of Adsorbed oxygen ions is decreased and the resistance decrease as consequence of the reduction in both surface potential barrier height and the depletion range [12, 21-22, 35, 37].

Conclusion

In conclusion, the XPS depth profile investigations on SnO₂ modified with Cu have proven to be a useful tool toward better understanding of sensing mechanisms of CO, H₂ and

LPG gas. The sensitivity of SnO₂:Cu sensors is shown to depend on the work function of the metal additive. The gas sensing characteristics and the XPS valence band studies both indicate that the gas sensitivity of the sensor increases with the work function of the additive concentration. The core level studies give some very interesting observations and conform the sensitization mechanism in SnO₂:Cu (O) to be purely chemical and largely electronic. The core levels of Sn and O in SnO₂:Cu (O) show a shift in the binding energy as compared to virgin SnO₂ with change in additive concentration. This has been attributed to increase in the surface work function because of the incorporation of the proper additive concentration (Cu = 9 wt. %). The enhancement of CO dissociation with effect of material sintering temperature is observed CO interaction with SnO₂:Cu (O) leads to formation of carboxylate like O-C-O species. The addition of Cu enhances the CO dissociation via CO surface by an electronics effect of a semi conducting material interaction. CO exposure at optimum operating temperature results in CO dissociation and carbon contamination of the surface.

Acknowledgements

One of the authors Dr. P.S. More would like to thank UGC for financial support. The research was primarily supported by UGC. Dr. D. J. Late would like to thank DST (Government of India) for Ramanujan Fellowship and Partial support by DST Fast-Track project Grant No. SB/FT/CS-116/2013 is gratefully acknowledged.

Reference

- Dawit, G.; Paulowicz, I.; Kaps, S.; Lupan, O.; Wille, S.; Haidarschin, G.; Mishra, Y. K.; Adelong R.; *Advanced Materials*, **2014**, 26, 1541.
DOI: [10.1002/adma.201304363](https://doi.org/10.1002/adma.201304363)
- Mishra, Y. K.; Kaps, S.; Schuchardt, A.; Paulowicz, I.; Jin, X.; Gedamu, D.; Freitag S.; Claus, M.; Wille, S.; Kovalev, A.; Gorb, S. N.; Adelong R.; *Part. Part. Syst. Charact.* **2013**, 30, 775.
DOI: [10.1002/ppsc.201300197](https://doi.org/10.1002/ppsc.201300197)
- Mishra, Y. K.; Modi, G.; Vasiliu C.; Vasile P.; Oleg L.; Tim R.; Ingo P.; Viktor H.; Wolfgang B.; Lorenz K.; Rainer A.; *ACS Appl. Mater. Interfaces* **2015**, 7, 14303.
DOI: [10.1021/acsami.5b02816](https://doi.org/10.1021/acsami.5b02816)
- Paulowicz, I.; Viktor H.; Soren K.; Vasiliu C.; Oleg L.; Tudor B.; Viola D.; Ion T.; Lorenz K.; Rainer A.; Yogendra K. M.; *Advanced Electronic Materials* **2015**, 1.
DOI: [10.1002/aelm.201500081](https://doi.org/10.1002/aelm.201500081)
- Lupan, O.; Tudor B.; Mao D.; Lidia G.; Ingo P.; Yogendra K. M.; Lorenz K.; Rainer A.; Ion T.; *Sens. Actuators, B* **2015**, 221, 544.
DOI: [10.1016/j.snb.2015.06.112](https://doi.org/10.1016/j.snb.2015.06.112)
- Chen, J.; Lina X.; Weiyang L.; Xing-long G.; *Advanced Materials* **2005**, 17, 582.
DOI: [10.1002/adma.200401101](https://doi.org/10.1002/adma.200401101)
- Yang, S.; Zhao W.; Yongming H.; Xiantao L.; Jinmei L.; Di Z.; Linfeng F.; Yu W.; Haoshuang G.; *ACS applied materials & interfaces* *ACS Appl. Mater. Interfaces*, **2015**, 7, 9247.
DOI: [10.1021/acsami.5b01858](https://doi.org/10.1021/acsami.5b01858)
- Volanti, D. P.; Anderson A. F.; Pedro H. S.; Elson L.; Jose A. V.; Marcelo O. O.; *Physical Chemistry Chemical Physics* **2015**, 17, 18761.
DOI: [10.1039/C5CP02150B](https://doi.org/10.1039/C5CP02150B)
- Lu, Y.; Ma, Y. H.; Ma, S. Y.; Jin, W. X.; Yan, S. H.; Xu, X. L.; Jiang X. H.; Wanga, T. T.; Yanga, H. M.; Chena, H.; Qianga Z.; *Materials Letters* **2015** (In Press).
DOI: [10.1016/j.matlet.2015.10.117](https://doi.org/10.1016/j.matlet.2015.10.117)
- Pawar, M. S.; Bankar, P. K.; More, M. A.; Late, D. J.; *RSC Advances* **2015**, 5, 88796.
DOI: [10.1039/C5RA17253E](https://doi.org/10.1039/C5RA17253E)
- Zotti, A.; Zuppolini, S.; Giordano, M.; Zarrelli, M.; Borriello, A.; De Luca, G.; *AISEM Annual Conference, 2015 XVIII*, pp. 1-3. IEEE, **2015**.
DOI: [10.1109/AISEM.2015.7066832](https://doi.org/10.1109/AISEM.2015.7066832)
- Ma, N.; Suematsu K.; Masayoshi Yuasa, and Kengo Shimanoe. "Pd Size Effect on the Gas Sensing Properties of Pd-Loaded SnO₂ in Humid Atmosphere." *ACS applied materials & interfaces* **2015**, 7, 15618.
DOI: [10.1021/acsami.5b04380](https://doi.org/10.1021/acsami.5b04380)
- Saito, S.; Masaru M.; Kunihito K.; Hiroaki Y.; *Journal of the American Ceramic Society* **1985**, 68, 40.
- Kuang, Q.; Changshi L.; Zhong L. W.; Zhaoxiong X.; Lansun Z.; *Journal of the American Chemical Society* **2007**, 129, 6070.
DOI: [10.1021/ja070788m](https://doi.org/10.1021/ja070788m)
- Chen, Y. J.; Xue, X. Y.; Wang, Y. G.; Wang, T. H.; *Applied Physics Letters* **2005**, 87, 233503.
DOI: [10.1063/1.2140091](https://doi.org/10.1063/1.2140091)
- Sun, P.; Wan Z.; Yang C.; Yue G.; Yanfeng, S.; Geyu L.; *Cryst Eng Comm* **2011**, 13, 3718.
DOI: [10.1039/C1CE05073G](https://doi.org/10.1039/C1CE05073G)
- Wang, H.; Qingqin L.; Weijie W.; Yiran A.; Jinghong L.; Lin G.; *Crystal Growth & Design* **2011**, 11, 2942.
DOI: [10.1021/cg2001255](https://doi.org/10.1021/cg2001255)
- Joseph, J.; Mathew, V.; Abraham. K. E.; *Crystal Research and Technology* **2006**, 41, 1020.
DOI: [10.1002/crat.200610714](https://doi.org/10.1002/crat.200610714)
- Chiodini, N. A.; Paleari, D.; Martino, D.; Spinolo, G.; *Applied physics letters* **2002**, 81, 1702.
DOI: [10.1063/1.1503154](https://doi.org/10.1063/1.1503154)
- Zhong, Z.; Yin, Y.; Gates, B.; Xia, Y.; *Advanced Materials* **2000**, 12, 206.
- More, P.S.; Kholam, Y. B.; Deshpande, S. B.; Sainkar, S. R.; Date, S. K.; Karekar R. N.; Aiyer, R. C.; *Mater. Lett.* **2003**, 57, 2177.
DOI: [10.1016/S0167-577X\(02\)01170-9](https://doi.org/10.1016/S0167-577X(02)01170-9)
- More, P.S.; Kholam, Y.B.; Deshpande, S.B.; Sainkar, S. R.; Date, S. K.; Karekar, R. N.; Aiyer, R. C.; *Mater. Lett.* **2003**, 58, 205.
DOI: [10.1016/S0167-577X\(03\)00446-4](https://doi.org/10.1016/S0167-577X(03)00446-4)
- Lantoo V.; Rampainen P.; *J. Electrochem. Soc.*, **1998**, 135, 2550.
DOI: [10.1149/1.2095378](https://doi.org/10.1149/1.2095378)
- Jun, Seok-Taek.; choi, G. M.; *J. Am. Ceram. Soc.* **1998**, 81, 695.
DOI: [10.1111/j.1151-2916.1998.tb02391.x](https://doi.org/10.1111/j.1151-2916.1998.tb02391.x)
- Wilman, D.F.; Vondel, V. d.; and Vander Kelen, G. P.; *Inorg. Chem Acta.* **1979**, 34, 175.
DOI: [10.1016/S0020-1693\(00\)94698-X](https://doi.org/10.1016/S0020-1693(00)94698-X)
- Toyoshima, Somorjai, G.A.; *Catal Rev. Sci-Eng.* **1979**, 19, 105.
DOI: [10.1080/03602457908065102](https://doi.org/10.1080/03602457908065102)
- Kurt W. Kolasinski [eds] "Surface Science" John Wiley and Sons LTD **2001**.
DOI: [978-0-470-03304-3](https://doi.org/10.1002/978-0-470-03304-3)
- Boyle J. F.; Jones, K. A.; *J. Electron Mater.* **1977**, 6, 356.
- Kamp, B.; Merkle, R.; Maier J.; *Sens. Actuators, B* **2001**, 77, 534.
DOI: [10.1016/S0925-4005\(01\)00694-3](https://doi.org/10.1016/S0925-4005(01)00694-3)
- Moseley, P. T.; *Meas. Sci. Technology* **1997**, 8, 223.
DOI: [10.1088/0957-0233/8/3/003](https://doi.org/10.1088/0957-0233/8/3/003)
- Gopel, W.; Schierbaum, K.D.; *Sens. Actuators, B.* **1995**, 26, 1.
DOI: [10.1016/0925-4005\(94\)01546-T](https://doi.org/10.1016/0925-4005(94)01546-T)
- Phani, R.; Manorama, S.; Rao, V. J.; *J. Phys. Chem. Solids.* **2000**, 61, 985.
DOI: [10.1016/S0022-3697\(99\)00215-2](https://doi.org/10.1016/S0022-3697(99)00215-2)
- Morazzoni, F.; Canevali, C.; Chiodini, N.; Mari, C.; Ruffo, R.; Scott, R.; Armelao, L.; Tondello, E.; Depero, L.; *Mater. Sci. Eng. C* **2001**, 15,167.
DOI: [10.1016/S0928-4931\(01\)00255-7](https://doi.org/10.1016/S0928-4931(01)00255-7)
- Ghijssen, L. H.; Tjeng, J.; van E.; Eskes, H.; Westerink, J.; Sawatzky, A.; *Phys. Rev. B.* **1998**, 38,11322.
DOI: [10.1088/0957-4484/23/19/194014](https://doi.org/10.1088/0957-4484/23/19/194014)
- Rao, C. N. R.; Raju A. R.; Vijayamohan K.; "Gas -Sensor Materials" New Materials, ed Nagakura S. (Narosa Pub. House, New Delhi) **1992**.
- David, F.C.; Fryberger, T.; Semancik, S.; *Phys. Rev. B.* **1988**, 38, 3.
DOI: [10.1103/PhysRevB.38.2072](https://doi.org/10.1103/PhysRevB.38.2072)
- Kawabe, T.; Tabata, K.; Suzuki, E.; Yamaguchi, Y.; Nagasawa, Y.; *J. Phys. Chem. B.* **2001**, 105, 4239.
DOI: [10.1021/jp003234d](https://doi.org/10.1021/jp003234d)
- Mathew, T.; Shiju, N.; Sreekumar, K.; Rao B.; Gopinath, C.; *J. Catalysis.* **2002**, 210, 405.
DOI: [10.1006/jcat.2002.3712](https://doi.org/10.1006/jcat.2002.3712)
- Manassidis, I.; Goniakowski, J.; Kantorovich, L. N.; Gillan., M. J. *Surface Science* **1995**, 339, 258.


- DOI: [0039-6028\(95\)00677-X](https://doi.org/10.1039/95000677X)
40. Velu, S.; Suzuki, K.; Gopinath, C.; Hattori T.; Yoshida, H.; *Physical Chemistry*. **2002**, *4*, 1990.
DOI: [10.1039/b109766k](https://doi.org/10.1039/b109766k)
41. Vijayaraj M.; and Gopinath, C.S.; *J. Catalysis* **2006**, *241*, 83.
DOI: [10.1016/j.jcat.2006.04.010](https://doi.org/10.1016/j.jcat.2006.04.010)
42. Gopel, W.; Schierbaum, K.; *Sens. Actuators, B*. **1995**, *26*, 1.
DOI: [10.1016/0925-4005\(94\)01546-T](https://doi.org/10.1016/0925-4005(94)01546-T)
43. Sergio Moreno, M.; Punte, G.; Rigotti, G.; Mercader, R.; *Solid State Ionic* **2001**, *144*, 81.
DOI: [10.1016/S0167-2738\(01\)00882-7](https://doi.org/10.1016/S0167-2738(01)00882-7)
44. Galdikas, A.; Jasutis, V.; Kaciulis, S.; Mattogno, G.; Mironas, A.; Olevano, V.; Senuliene, D.; Setkus, A.; *Sens. Actuators, B.*, **1997**, *43*, 140.
DOI: [10.1016/S0925-4005\(97\)00206-2](https://doi.org/10.1016/S0925-4005(97)00206-2)

Advanced Materials Letters


Copyright © 2016 VBRI Press AB, Sweden
www.vbripress.com/aml

Publish your article in this journal

Advanced Materials Letters is an official international journal of International Association of Advanced Materials (IAAM, www.iaamonline.org) published monthly by VBRI Press AB from Sweden. The journal is intended to provide high-quality peer-review articles in the fascinating field of materials science and technology particularly in the area of structure, synthesis and processing, characterisation, advanced-state properties and applications of materials. All published articles are indexed in various databases and are available download for free. The manuscript management system is completely electronic and has fast and fair peer-review process. The journal includes review article, research article, notes, letter to editor and short communications.



VBRI Press
a rapid publication platform



A Monthly Journal